BNL 20437
CONF-750629--5

MASTER

Multilayer Monochromators for Neutron Scattering

A. M. SAXENA AND B. P. SCHOENBORN

Biology Department, Brookhaven National Laboratory, Upton, New York 11973

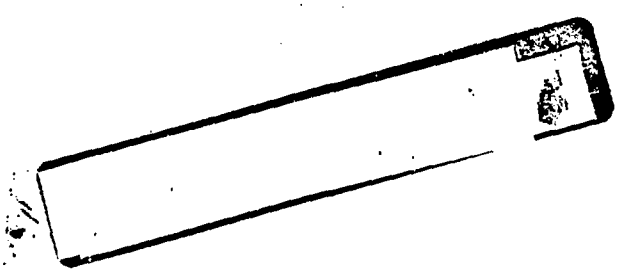

MASTER

INTRODUCTION

In an earlier paper Schoenborn, Caspar and Kammerer[1] have reported the fabrication of thin film monochromators for neutrons. They had shown that a multilayer consisting of alternating films of two materials acts as a good monochromator with large and adjustable periodicity and wide bandwidth.

The diffraction properties of these multilayers have been studied with the objective of using them as monochromators, filters and polarizers for neutrons. A theoretical understanding of these multilayers has been developed by using the kinematical and dynamical approaches. In order to compare these expressions with the observed properties, the effects of beam divergence and wavelength distribution for the spectrometer have been determined. The influence of some aperiodicity on the diffraction data has also been studied within the framework of kinematical theory.

Sample preparation

The materials selected for making the multilayers should possess a number of properties. A large difference in neutron scattering amplitude density, f, defined as $f = b\rho$ where b = scattering length per atom and ρ = number of nuclei per unit volume, gives rise to a greater contrast in scattering parameters and hence larger intensity for a given number and thickness of bilayers in the samples. Values of f for some of the elements are listed in Table 1. The difference between scattering densities of the two materials can be increased by choosing one material with a negative scattering length and the other with a positive scattering length. In addition to this, the materials

selected should form uniform thin films and should have small interdiffusion. On the basis of these considerations it was decided to make multilayers of manganese and germanium. Manganese is one of the few elements with a negative scattering length, and the interdiffusion between these two materials is fairly small.

The multilayers were made by depositing thin films of Mn and Ge on a flat glass substrate by vacuum deposition technique.[2] Manganese and germanium were placed in boats of tantalum and graphite respectively, and were evaporated in succession by resistive heating of the boats. The thicknesses of the films were measured by a quartz crystal oscillator which also opened and closed a shutter at preset values through an automatic control unit. During the time that one material was being evaporated, the other was kept slightly below its melting point so that the time interval between depositing films was fairly small.

Thicknesses of all the films in a good multilayer should be identical with deviations not exceeding a few per cent. In order to achieve this it was necessary to work with low evaporation rates, a typical value being 1 Å/sec. At low evaporation rates the films are contaminated with some oxygen and carbon. The composition of different sections of a multilayer was determined by Auger spectroscopy and the contamination was, in general, found to be less than 1%. Most of the multilayers were made by depositing the films on a substrate held at room temperature. The size of the substrates used was 2.5 cm x 15 cm and they were kept at about 70 cm from the boats to ensure uniformity in the thickness of each film.

Multilayers with periodicity ranging from 120 Å to 240 Å have been made and a maximum of 75 bilayers were deposited on a multilayer. The maximum number of bilayers on a sample was limited by the capacity of the boats. For our geometry, the amount of material needed to make a multilayer with 75 bilayers and a periodicity of 200 Å was of the order of 8 g.

THEORY

(A) Kinematical theory

According to the kinematical theory, the differential scattering cross-section for a multilayer may be written as[3]

$$\frac{d\sigma}{d\Omega} = C \mid F \mid^2 \qquad (1)$$

where F is the structure factor for the multilayer and C is a constant. Let $\vec{K}$ be the incident wave vector and $\vec{K}'$ the scattered wave vector. For Bragg reflection from the multilayer the scattering vector is

$$\vec{Q} = \vec{K} - \vec{K}' = \frac{4\pi}{\lambda} \sin\theta \ \vec{z} \qquad (2)$$

where θ is the angle of incidence of the neutron wave on the multilayer and $\vec{z}$ is a unit vector perpendicular to the plane of the multilayer as shown in Fig. 1. λ is the wavelength of the incident neutron beam. The structure factor may be calculated for any given distribution of thicknesses and materials inside the multilayer.

It will be assumed that the composition of layers changes discretely along the z-axis and that the thickness of each layer is $d/2$ which gives rise

to a periodicity of d. Let b_1 and b_2 be the scattering lengths for the two materials and ρ_1, ρ_2 their nuclear densities. Then the structure factor is

$$F = \sum_{p=1}^{N} \{b_1\rho_1 \int_{(p-1)d}^{(p-\frac{1}{2})d} e^{iQz}\, dz + b_2\rho_2 \int_{(p-\frac{1}{2})d}^{pd} e^{iQz}\, dz\}$$

where N is the total number of bilayers. The above expression may be simplified to give

$$F = \frac{2\sin(Qd/4)}{Q} \cdot \frac{\sin(QNd/2)}{\sin(Qd/2)} \times [b_1\rho_1\, e^{iQd(\frac{N}{2}-\frac{1}{4})} + b_2\rho_2\, e^{iQd(\frac{N}{2}+\frac{1}{4})}$$

Since the scattered intensity is proportional to $|F|^2$, by multiplying this structure factor by its complex conjugate one obtains

$$|F|^2 = \{\frac{2\sin(Qd/4)}{Q} \frac{\sin(QNd/2)}{\sin(Qd/2)}\}^2 \times [(b_1\rho_1)^2 + (b_2\rho_2)^2 + 2b_1\rho_1 b_2\rho_2 \cos(Qd/2)] \quad (3)$$

For the nth order Bragg reflection $Q = (\frac{2\pi}{d})n$ and Eq. (3) simplifies to

$$|F|_B^2 = (\frac{Nd}{n\pi})^2 [b_1\rho_1 - b_2\rho_2]^2 \quad \text{for } n = 1,3,5....$$

$$|F|_B^2 = 0 \quad \text{for } n = 2,4,6.... \quad (4)$$

Therefore even order reflections will be absent because the net diffracted intensity from each layer is zero.

So far a sharp boundary between the materaisl has been considered. For an actual sample, however, the boundary between the layers is not expected to be discrete for two different reasons. First, there will be a certain amount of diffusion of materials between the layers. Second, any nonuniformity in the

surface of the sample will also have the same effect because the observed intensity is the total intensity scattered by the entire area of the sample which is exposed to the neutrons. A surface nonuniformity will cause displacement of some portion of the bilayer with respect to the rest along $\vec{z}$ direction, which is equivalent to partial mixing of the layers. The observed intensity for all the samples decreases rapidly for higher orders which also suggests that some mixing of materials is taking place.

The structure factor will also be calculated for the case in which the scattering amplitude density changes continuously in a sinusoidal way. In this case the nuclear scattering amplitude density may be written as

$$f_1 = \tfrac{1}{2} b_1\rho_1 (1 + \sin g z)$$
$$f_2 = \tfrac{1}{2} b_2\rho_2 (1 - \sin g z) \qquad (5)$$

where $g = 2\pi/d$. The structure factor now becomes

$$F = \tfrac{1}{2} b_1\rho_1 \int_o^{Nd} (1 + \sin g z)\, e^{iQz}\, dz + \tfrac{1}{2} b_2\rho_2 \int_o^{Nd} (1 - \sin g z)\, e^{iQz}\, dz$$

$$= e^{iQNd/2} \sin (QNd/2) \left\{\frac{1}{Q^2} (b_1\rho_1 + b_2\rho_2) + \frac{ig}{Q^2-g^2} (b_1\rho_1 - b_2\rho_2)\right\}$$

From this we obtain

$$|F|^2 = \sin^2 \left(\frac{QNd}{2}\right) \left\{\frac{1}{Q^2} (b_1\rho_1 + b_2\rho_2)^2 + \frac{g^2}{Q^2-g^2} (b_1\rho_1 - b_2\rho_2)^2\right\} \qquad (6)$$

For first order Bragg peak this structure factor gives

$$|F|_B^2 = \frac{1}{16} N^2 d^2 (b_1\rho_1 - b_2\rho_2)^2 \qquad (7)$$

while $|F|^2$ is zero for all higher order Bragg reflections.

(B) Dynamical theory

The underlying assumption in kinematical theory is that the intensity of the incident beam is uniform throughout the sample. Because of this assumption, the reflected intensity is proportional to the square of the number of bilayers and does not have an upper bound. Actually, however, the intensity of the incident beam will decrease as it goes deeper inside the sample because part of the incident beam is reflected by the upper layers. In addition, a proper theoretical approach should consider the multiple reflections of neutrons inside the multilayer as well.

These factors may be taken into account by solving the wave equation for a finite one-dimensional periodic medium with appropriate boundary conditions at the surfaces. The procedure of Zachariasen[4] will be followed after converting the variables to those for neutron waves. The reflected intensity near the Bragg peak is given by

$$\frac{P_H}{P_o} = \frac{\sinh^2 [A\sqrt{1-y^2}]}{1-y^2+\sinh^2[A\sqrt{1-y^2}]} \qquad (8)$$

where

$$A = \frac{t_o |V_g|}{2\sqrt{|K_z(K_z-g)|}}$$

and

$$y = \left\{\frac{|K_z-g|}{|K_z|}\right\} \cdot \frac{1}{V_g}\left[\frac{K_z}{2(K_z-g)}(g^2-2g K_{oz}) - \frac{g V_o}{2(K_z-g)}\right]$$

and other symbols represent the following: $V_o = 2\pi(\rho_1 b_1 + \rho_2 b_2)$; $V_g = 2(\rho_1 b_1 - \rho_2 b_2)$; $t_o = Nd$ is the total thickness of the multilayer; K_z = the z component

of the neutron wave vector inside the multilayer; K_{oz} = the z component of the neutron wave vector outside the multilayer. At the Bragg angle $y = 0$, and the diffracted intensity is

$$\frac{P_H}{P_o} = \tanh^2(A)$$

with

$$A = \frac{t_o |V_g|}{2|K_z|} \qquad (9)$$

This equation appropriately shows saturation of P_H/P_o for large t_o.

(C) Effect of finite resolution of spectrometer

The diffraction pattern of the system will also be modified due to finite beam divergence and wavelength distribution of the spectrometer. The experimental setup is shown in Fig. 2. The incident neutron beam has traversed through a polycrystalline beryllium filter and therefore consists of a continuous distribution of wavelengths with a low angle cut off at 3.9 Å. The intensity of various wavelength components decreases uniformly from about 4 Å with negligible intensity for wavelengths greater than 6 Å. This distribution may be determined by taking a θ-2θ plot of the incident beam and applying suitable corrections for beam divergence. The wavelength composition of the primary beam will be represented by $I^o(\lambda)$ and assumed to be known.

The divergence of the incident beam will be determined by the collimating slits used. Since the multilayer intercepts only a small portion of the incident beam, collimation was achieved by passing the neutron beam through two slits. For most of the experiments the beam width was 0.30 mm and the beam divergence was 1 milliradian.

The scattered beam from the sample passes through Soller slits and is then incident on an analyzer crystal. The wavelength distribution of the neutrons reaching the detector is determined by the mosaic spread of the analyzer.

The procedure employed for taking the resolution function into account is based on tracing the path of a general ray from the collimating slits to the detector. The net intensity is then obtained by integrating over the entire scattered beam. It will be assumed that the profile of a beam emerging from a set of slits is a Gaussian of known width. The validity of this assumption has been confirmed for the narrow slits employed in these measurements. The intensity of a ray making an angle δ with the axis of the slit is then decreased by a factor $e^{-K\delta^2}$ where K is the slit constant related to the width of the beam such that $FWHM = \sqrt{(\ln 2/K)}$. It will be assumed that K_1 and K_2 are the slit constants for the collimating slits and the Soller slits before the detector, respectively. The distribution of crystallites in the graphite analyzer has been shown to be Gaussian[5], so that the probability of finding a mosaic block making an angle β with the surface of the crystal is $e^{-K_3\beta^2}$. The constant K_3 was determined by analyzing the rocking curve of the crystal, and the constants K_1 and K_2 were obtained from an analysis of the direct beam profile as a function of the slit width. The values ascribed to these constants were: $K_1 = 2.3678\ 10^6$ $(\text{radian})^{-2}$; $K_2 = 1.6342\ 10^5$ $(\text{radian})^{-2}$; and $K_3 = 9.4\ 10^3$ $(\text{radian})^{-2}$.

As shown in Fig. 2, the path of the most probable ray coincides with the axes of the slits and is shown by a dashed line. The multilayer is set

along a bisector of the axes of collimating and Soller slits such that the mean ray is incident on it at an angle θ_o. The path of a general ray, which is incident at an angle θ on the multilayer, is shown by a solid line in this figure. The probability function affecting the intensity of the general ray at each stage will be calculated and combined to give the net intensity. The following notation will be used to denote the angles involved: θ_o = the angle of incidence of the most probable ray on the multilayer; θ = angle of incidence of a general ray on the multilayer; β = angle subtended by that mosaic block with the surface of the analyzer which reflects the general ray from the multilayer; $\Delta\theta$ = the difference in angles of the reflected and incident rays on the multilayer for the general ray; α = angle of incidence of the mean ray on the analyzer. This angle is related to the wavelength for which diffraction data is taken through Bragg relation $\lambda = 2d_G \sin\alpha$ where d_G is the d-spacing of the analyzer crystal. Also, ϵ_A = angle of incidence of the general ray on the crystallite β, Ψ = rocking angle for the multilayer such that $\Psi = 0$ corresponds to specular reflection of the mean ray.

Three different types of observations have been taken for each multilayer. For the θ-2θ plots the increment in angle for detector arm is twice that for multilayer. For the rocking curve, the detector arm is set at twice the Bragg angle while the multilayer is moved on both sides of the Bragg angle. Finally, for the reflectivity analysis the multilayer is mounted on axis "1" and a graphite crystal on axis "2". The usual analyzer is removed from "3" axis and the detector is rotated so that it directly faces the Soller

slits. While the multilayer is kept at a fixed angle with respect to the incident beam, the wavelength distribution of the reflected beam is determined by taking a θ-2θ plot with the analyzer. The effect of finite resolution of the spectrometer will have to be introduced in each type of scan.

(i) θ-2θ plot. The general ray, which is incident at an angle θ on the multilayer, emerges making an angle $\theta-\theta_o$ with the axis of the collimating slits. Therefore it is attenuated by a factor $e^{-K_1(\theta-\theta_o)^2}$ with respect to the most probable ray. The diffracted beam from the multilayer for this particular incident ray will be appreciable inside a narrow cone with its axis along the specularly reflected ray. The intensity of the wave diffracted at $\theta + \Delta\theta$ will then be proportional to the square of the structure factor, $|F(\theta|\theta + \Delta\theta)|^2$, calculated for this kind of reflection. Since the Soller slits on the detector side are set to receive the most probable ray, this particular ray will be further attenuated by a factor $e^{-K_2(\theta + \Delta\theta - \theta_o)^2}$ on passing through the Soller slits.

Finally, it will be assumed that this ray is reflected by a mosaic block of the analyzer which makes an angle β with the surface of the crystal as shown in the inset of Fig. 2. The probability of finding a mosaic block at an angle β is $e^{-K_3\beta^2}$. However, the incidence angle of this ray on the crystallite is $\epsilon = \alpha + \theta + \Delta\theta - \theta_o - \beta$. Therefore only that wavelength component of this ray will be reflected which satisfies the Bragg relation for this angle of incidence:

$$\lambda = 2d_G \sin(\alpha + \theta + \Delta\theta - \theta_o - \beta) \qquad (10)$$

Each mosaic block will reflect the wavelength satisfying the above relation and the distribution of wavelengths reaching the detector is determined by the angular distribution of mosaic blocks.

The total intensity reaching the detector is obtained by integrating over appropriate ranges of: a) θ, to include beam divergence; b) $\Delta\theta_o$ to take care of waves not reflected specularly from the multilayer; c) λ, to include all wavelength components of the primary beam; and d) β, to include the distribution of mosaic blocks in the analyzer crystal. However, according to Eq. (10) λ and β are not independent variables and only one of these need to be integrated. Equation (10) may be rewritten as:

$$\beta = \alpha + \theta + \Delta\theta - \theta_o - \sin^{-1}(\lambda/2d_G) \tag{11}$$

The net intensity reaching the detector, aside from a multiplying constant, is then given by the following expression

$$I(\theta_o) = \iiint d\lambda \cdot d\theta \cdot d(\Delta\theta)\, [I^o(\lambda) \cdot e^{-K_1(\theta-\theta_o)^2}\, e^{-K_2(\theta + \Delta\theta - \theta_o)^2} \times e^{-K_3\beta^2}\, |\, F(\theta|\theta + \Delta\theta)\,|^2] \tag{12}$$

where β is given by Eq. (11). The integrals in Eq. (12) were evaluated by using Legendre-Gauss quadrature formula[6]. It was found that $\Delta\theta$ integration had negligible effect on the shape of $I(\theta_o)$. This showed that only specular reflections from the multilayer made a significant contribution. Therefore $I(\theta_o)$ may be written as a double integral

$$I(\theta_o) = \iint d\lambda \cdot d\theta\, [I^o(\lambda)\, e^{-(K_1 + K_2)(\theta-\theta_o)^2}\, e^{-K_3\beta^2}\, |\, F(\theta)\,|^2] \tag{13}$$

where $\beta = \alpha + \theta - \theta_o - \sin^{-1}(\lambda/2d_G)$. In all future considerations, the effects of nonspecular reflections from the multilayer will be neglected.

Figure 3 shows a plot of $|F|^2$ for N = 25 and d = 160 Å, and Fig. 4 is a plot of the calculated values of $I(\theta_o)$ from this $|F|^2$ and the constants of the spectrometer given above. It can be seen that while $|F|^2$ shows a large number of oscillations between Bragg peaks, all these features are smoothed out when the resolution function of the spectrometer is taken into account. By replacing $|F|^2$ by P_H/P_o of dynamical theory, one obtains the diffraction pattern of dynamical theory for a finite resolution function.

(ii) Rocking curve. The procedure for calculating various probability functions is identical to the one followed for θ-2θ plots. Ψ is the rocking angle which measures the angular deviation of the multilayer from the Bragg position, i.e. when the most probable ray is incident at the Bragg angle, θ_o, on the multilayer and the detector arm is set at twice the Bragg angle. θ is the angle of incidence of a general ray on the multilayer for the setting Ψ. The incidence angle of the general ray reflected from multilayer at Ψ on a mosaic block making an angle β with the surface of the analyzer is $\epsilon = \alpha + \theta_o - \Psi - \theta - \beta$. The net intensity on the detector for a setting Ψ of the multilayer is

$$I(\Psi) = \iint d\lambda \cdot d\theta \left[I^o(\lambda)\, e^{-K_1(\theta_o + \Psi - \theta)^2} |F(\theta)|^2\, e^{-K_2(\Psi + \theta - \theta_o)^2} e^{-K_3\beta^2} \right] \quad (14)$$

where $\beta = \alpha + \theta_o - \Psi - \theta - \sin^{-1}(\lambda/2d_G)$.

(D) Aperiodicity in multilayers

In the considerations so far it has been assumed that the multilayer is perfect in the sense that all the bilayers of a sample are exactly identical. Since a single monolayer of most materials is 3-4 Å thick, there will be some aperiodicity in all the samples. In addition to this, any surface undulations in the substrate will also give rise to an effective aperiodicity.

The bilayers in a multilayer are stacked on each other and therefore there is a definite phase relation in the waves diffracted by different bilayers. If a particular bilayer does not have the proper thickness then it makes a singular contribution to the diffracted wave and also alters the phase relation between the bilayers preceding it and succeeding it. Because of this fact, the diffraction properties will depend on the thicknesses of all the bilayers and their stacking sequence, and therefore exact expressions for these may be developed only if one knows the actual distribution of thicknesses in the multilayer.

For analyzing the experimental data a simple model has been considered in which the thickness of bilayers changes uniformly from one end of the sample to the other. This is a simplified model in which the distribution of aperiodicities is replaced by a single parameter. It is easy to calculate the structure factor for this case and obtain computed curves within the framework of kinematical theory. Because of the large number of variables which need to be determined for each sample, the exact approach using dynamical theory had been abandoned.

In the simplified model, each sample will be characterized by an aperiodicity parameter Δd such that $\delta = \Delta d/N$ is the (see text) thickness of the bilayer on which neutrons are incident from outside is d, then the thickness of the innermost bilayer will be $d + (N-1)\delta$. The pth bilayer will extend from $z = (p-1)d + \frac{1}{2}\delta(p-1)(p-2)$ to $z = pd + \frac{1}{2}\delta p(p-1)$, and the structure factor of this bilayer will be

$$F_p = \frac{2\sin(\epsilon_0 Q)}{Q}\left[\{b_1\rho_1 \cos(\epsilon_1 Q) + b_2\rho_2 \cos(\epsilon_2 Q)\} + i\{b_1\rho_1 \sin(\epsilon_1 Q) + b_2\rho_2 \sin(\epsilon_2 Q)\}\right] \tag{16}$$

where
$$\epsilon_0 = d + \tfrac{1}{2}(N-1)\delta$$
$$\epsilon_1 = (N-\tfrac{3}{2})d + \tfrac{1}{2}(N-1)(2N-3)\delta \tag{17}$$
$$\epsilon_2 = (N-\tfrac{1}{2})d + \tfrac{1}{2}(N-1)(2N-1)\delta .$$

The structure factor of the multilayer may therefore be written as

$$F = \sum_p \{\mathrm{Re}(F_p) + \mathrm{Im}(F_p)\}$$

hence

$$|F|^2 = \left[\sum_{p=1}^{N} \mathrm{Re}(F_p)\right]^2 + \left[\sum_{p=1}^{N} \mathrm{Im}(F_p)\right]^2 \tag{18}$$

where $\mathrm{Re}(F_p)$ and $\mathrm{Im}(F_p)$ are real and imaginary parts of F_p as given by Eq. (16). The structure factor of this model depends on the number of bilayers, d-spacing and the aperiodicity parameter, Δd. For a given value of these parameters, the computed θ-2θ plot and rocking and reflectivity curves can be obtained by substituting $|F|^2$ given by Eq. (18) and Eqs. (13), (14) and (15), respectively.

COMPARISON WITH EXPERIMENTS

(A) θ-2θ plots

A typical θ-2θ plot for a sample with N=25 and d=160 Å is shown in Fig. 5. As mentioned earlier, the diffraction properties are sensitive to the distribution of thicknesses in the multilayer and this will affect the θ-2θ plot as well.

The first intensity maximum at about 0.21° is due to critical angle reflection from glass substrate. A θ-2θ plot of the glass slide alone shows an intensity maximum at 0.21° with sharp decay beyond this angle. The solid curve for this region is the theoretical plot for critical angle reflection from glass. The intensity decreases for smaller angles as well because the entire incident beam is not intercepted by the glass slide. This low angle maximum can be eliminated by depositing the multilayer on a material with negative scattering length, such as titanium.

The first order Bragg peak for this ample is at 0.75°. The shape of this peak gives an idea about the quality of the sample. If the thickness of even a few bilayers is different from the rest by an appreciable amount, then one will end up with a Bragg peak which has prominent shoulders and even multiple peaks. An example of such a sample is shown in Fig. 6. It is worthwhile to point out that in the extreme case when a single layer from the middle of the multilayer is missing, the kinematical theory predicts zero intensity at the angle where Bragg condition is satisfied with intensity maxima on either side.

The second order Bragg peak for this sample (Fig. 5) has an intensity about 1/200 of the first order Bragg peak. For most of the samples the second order maximum is fairly weak but for a sample with large aperiodicities it may have appreciable intensity. Third and higher orders are hardly distinguishable from the background.

(B) Determination of Δd

For each sample the equivalent Δd of the simplified aperiodicity model was determined by comparing the rocking curve of the sample with the calculate one using Eqs. (18) and (14). Δd was used as a variable in Eq. (18) and its value for the best fit with experimental data was determined. Each sample was then characterized with this parameter. It may be pointed out that this method is similar to the determination of mosaic spread of a real crystal by an analysis of its rocking curve, but the significance of Δd is different because of phase relations between different bilayers. A comparison of this type is shown in Fig. 7 for a sample with N=25 and d=160 Å in which the solid curve has been calculated for Δd = 25 Å. This value of Δd is then used for comparing the reflectivity and θ-2θ plots with the calculated curves. The solid curve in θ-2θ plot, Fig. 5, uses this value of Δd. When the number of bilayers is less than 30, the calculated curves agree with the experimental data for the same value of Δd.

(C) Reflectivity of samples

According to kinematical theory the reflectivity of samples with the same d-spacing should be proportional to N^2 as given in Eq. (4). This leads to

the nonphysical result that the reflectivity does not have an upper bound. The dynamical theory, Eq. (9), takes care of this and the normalized intensity tends asymptotically to unity. Figure 8 shows these two plots for a periodicity of 160 Å. These are applicable, however, only to perfect samples and a spectrometer with infinite resolution.

If the finite resolution of the spectrometer is taken into account, the intensity predicted by the kinematical theory will be less than that for ideal geometry. The reason for this is that the FWHM of the Bragg peak decreases with increasing number of bilayers while the spectrometer measures the integrated intensity over finite angular range because of the beam divergence, and this integrated intensity will be less than the peak intensity by an amount dependent on the width of the peak. This effect becomes more and more pronounced as the number of bilayers is increased.

In Fig. 9 calculated curves for multilayers of two periodicities are shown along with the observed reflectivities. The solid curves (a) and (c) represent the results of kinematical theory for d-spacings of 160 Å and 220 Å, respectively. The dashed curves (b) and (d) have been calculated using the aperiodicity model. For curve (b), d=160 Å and Δd = 25 Å, while for (d), d = 220 Å and Δd = 35 Å. The reflectivities obtained for samples of 160 Å periodicity are shown by solid circles and those of 220 Å periodicity are shown by solid triangles. There is a fair agreement between calculated plots and experimental values for small values of N. For larger number of bilayers, the theoretical reflectivities continue to increase while the data points show saturation.

It would be worthwhile to emphasize that a complete understanding of a multilayer will require a knowledge of 2 N variables because the thicknesses and stacking order of the layers determine its diffraction properties and therefore a model with one variable, Δd, can only give a qualitative understanding. Because of the sensitiveness to so many variables, the reflectivities of two samples with the same N and d may be widely different. The situation is further complicated by the fact that there may be surface irregularities on the substrate and nonuniformities in the surfaces of the films.

The bandwidth, $\Delta\lambda/\lambda$, for most of these samples lies between 0.06 and 0.20. It can be shown that the lower limit of $\Delta\lambda/\lambda$ will be determined by the incidence angle on the sample and beam divergence of the spectrometer. The upper limit of $\Delta\lambda/\lambda$ is determined essentially by $\Delta d/d$ and, if necessary, it can be increased by introducing some aperiodicity in the multilayer during deposition. Figure 10 shows reflectivity plot for a sample with $\Delta\lambda/\lambda = 0.10$.

OSCILLATION DATA

The plot of $|F|^2$ in Fig. 3 shows oscillation between Bragg peaks of various orders. These intensity variations arise because the diffracted waves from different bilayers interfere to give undulations in intensity. It can be easily shown that for N bilayers there will be (N-1) minima between Bragg peaks of successive orders. If the period of oscillations is smaller than the beam divergence, the observed intensity will not show any oscillations because it will be integrated over more than a period.

An attempt was made to observe these oscillations by increasing the period of oscillations and decreasing the angular divergence of the incident beam. The period of oscillation for a sample is approximately $(\lambda/2Nd)$ and therefore one must decrease the total number of bilayers and periodicity. However, decreasing Nd also decreases the intensity of reflections and therefore a compromise must be made to get observable intensities. The data shown in Fig. 11 was taken for a sample with 10 bilayers and a periodicity of 180 Å. The beam width was reduced to 0.06 mm and the beam divergence to 0.24 milliradians for taking these observations. In the same figure $|F|^2$ for this sample has also been plotted after introducing the effects of finite resolution. The data clearly shows oscillations of the expected periodicity.

The fact that these oscillations are observed suggests that the coherence length of neutron wave packets is at least of the order of the total thickness of the multilayer because at an intensity minimum there is destructive interference between waves diffracted from different bilayers. From the observations of oscillations we conclude that the coherence length is at least of the order of 2000 Å. By observations of the diffraction pattern of a single slit, Shull[7] has shown that the coherence length of the neutron wave packets is at least of the order of 21 μ.

POLARIZING MULTILAYERS

Multilayers which polarize a beam of neutrons on reflection have also been made.[8] For this purpose a multilayer with alternating layers or iron and germanium was constructed and placed in a magnetic field of about 300 Oe which

saturates the magnetization of iron. In a magnetic field, the scattering from iron has a contribution from magnetic scattering in addition to the nuclear scattering. Since the magnetic moment has the direction of the external field, the nuclear scattering density seen by the neutron depends on whether its spin is parallel or antiparallel to the magnetic field. The values of nuclear scattering densities for the two spins of iron are 0.30×10^{11} and 1.32×10^{11} cm^{-2} while for germanium it has the value 0.37×10^{11} cm^{-2}. The result of this is that neutrons of one spin are reflected from the multilayer while the other spin-component moves in a medium of homogeneous scattering density.

An Fe-Ge multilayer with N = 32 and d = 165 Å was found to reflect 46% of the incident beam. The polarizability of the reflected beam, defined as

$$P = \frac{I^+ - I^-}{I^+ + I^-}$$

where I^+ and I^- are the intensities of the two spin components, was found to be 0.99. These figures suggest that one can make very efficient polarizers for neutrons using multilayers of this type.

DISCUSSION

The multilayers offer a number of advantages over conventional monochromators. The reflectivities of these multilayers are very good; by depositing enough layers one can make a multilayer with ~90% reflectivity. The number of bilayers required for this depends on the periodicity of the sample. For a periodicity of 220 Å a good multilayer with N = 40 can have

90% reflectivity, while for a periodicity of 120 Å about 200 bilayers will be required to get comparable reflectivity.

Because of their smaller take-off angle and inherent aperiodicity, the bandwidth $\Delta\lambda/\lambda$ for these samples is large and adjustable within some limits. For applications in which a greater $\Delta\lambda/\lambda$ is useful, such as low angle scattering from biological samples, this will lead to considerably greater intensities for the neutron beams. Finally, for long wavelength neutrons from cold source, for which almost no monochromators are available, the multilayers can be used as efficient monochromators.

The size of a multilayer required to reflect a neutron beam is determined by the Bragg angle for the selected wavelength, which in turn depends on the d-spacing. With our present setup in which films are made by resistive heating and deposited on a substrate held at room temperature, we have made good multilayers with smallest periodicity of 120 Å. With refined techniques it may be possible to push this limit down to 60 Å. For a d-spacing of 80 Å a multilayer will have to be 50 cm long in order to reflect a 12 mm wide beam of 4 Å wavelength. Making uniform films of this length will require different evaporation techniques, probably using sputtering for making the films. One may also have to investigate the combination of materials which gives uniform films of smallest thickness without any interdiffusion.

In addition to their use as monochromators and analyzers, the multilayers may also be used as filters for decreasing the intensity of the $\lambda/2$ component which gives rise to diffraction maxima at the same angles as the

wavelength λ for which the observations are being made. Because the intensity of the second order peak is less than the intensity of the first order Bragg peak by more than two orders of magnitude, a multilayer monochromator will automatically act as a filter as well. Additional filtering may be achieved by arranging a number of multilayers in transmission or reflection geometry.

Acknowledgements--Research carried out at Brookhaven National Laboratory under the auspices of the U. S. Energy Research and Development Administration. The authors are indebted to Dr. M. Strongin for his help in preparing the multilayers, Dr. M. Blume for suggesting the approach to kinematical theory, and to Dr. S. Mendiratta for helping us with the dynamical theory. The help given by Dr. G. Zaccai in initiating this work is also gratefully acknowledged.

REFERENCES

1. SCHOENBORN, B. P., CASPAR, D. L. D. AND KAMMERER, O. F., J. Appl. Cryst. 7, 508-510 (1974).

2. CHOPRA, K. L., Thin Film Phenomena, McMillan, New York, 1969.

3. MARSHALL, W. AND LOVESEY, S. W., Theory of Thermal Neutron Scattering, Oxford University Press, Oxford, 1971.

4. ZACHARIASEN, W. H., Theory of X-ray Diffraction in Crystals, John Wiley & Sons, New York, 1945.

5. SAXENA, A. M. AND SCHOENBORN, B. P., in preparation.

6. HILDEBRAND, F. B., Introduction to Numerical Analysis, McGraw-Hill, New York, 1956.

7. SHULL, C. G., Phys. Rev. 179, 752-754 (1969).

8. KJEMS, J. K., LYNN, J. W., PASSELL, L., SAXENA, A. M., AND SCHOENBORN, B. P., in preparation.

Table 1

Neutron Scattering Amplitude Density

for Some Elements

Element	b (10^{-12} cm)	f (10^{11} cm)
Al	0.35	0.21
Ti	-0.34	-0.19
Mn	-0.36	-0.29
Ni	1.03	0.94
Cu	0.79	0.67
Ge	0.84	0.37
Ag	0.61	0.36
Pb	0.96	0.32

FIGURE LEGENDS

Figure 1. Cross section of a multilayer.

Figure 2. Schematic diagram of the spectrometer. The inset shows a mosaic block of analyzer which participates in reflection.

Figure 3. Square of the structure factor vs. the angle of incidence on the sample.

Figure 4. $|F|^2$ after introducing the effect of resolution of the spectrometer.

Figure 5. θ-2θ plot for a sample with N = 25, d = 160 Å. The solid curve for $\theta < 0.3^\circ$ has been calculated for critical angle reflection from glass, and for $\theta > 0.3^\circ$ it has been calculated from the aperiodicity model with Δd = 25 Å.

Figure 6. θ-2θ plot for a sample with N = 37 and d = 200 Å.

Figure 7. Rocking curve for a sample with N = 25 and d = 160 Å. Δd = 25 Å for the solid curve.

Figure 8. Theoretical reflectivities for d = 160 Å. Solid curve represents kinematical theory and the dashed curve shows results of dynamical theory.

Figure 9. Theoretical reflectivity curves and experimental data points. Curves (a), (b) and solid circles are for d = 160 Å, and (c), (d) and solid triangles are for d = 220 Å.

Figure 10. Reflectivity plot for a sample with N = 10, d = 220 Å. Δd = 35 Å for the solid curve.

Figure 11. θ-2θ plot for a sample with N = 10, d = 180 Å. The solid curve shows integral of $|F|^2$ over beam divergence and wavelength distribution.

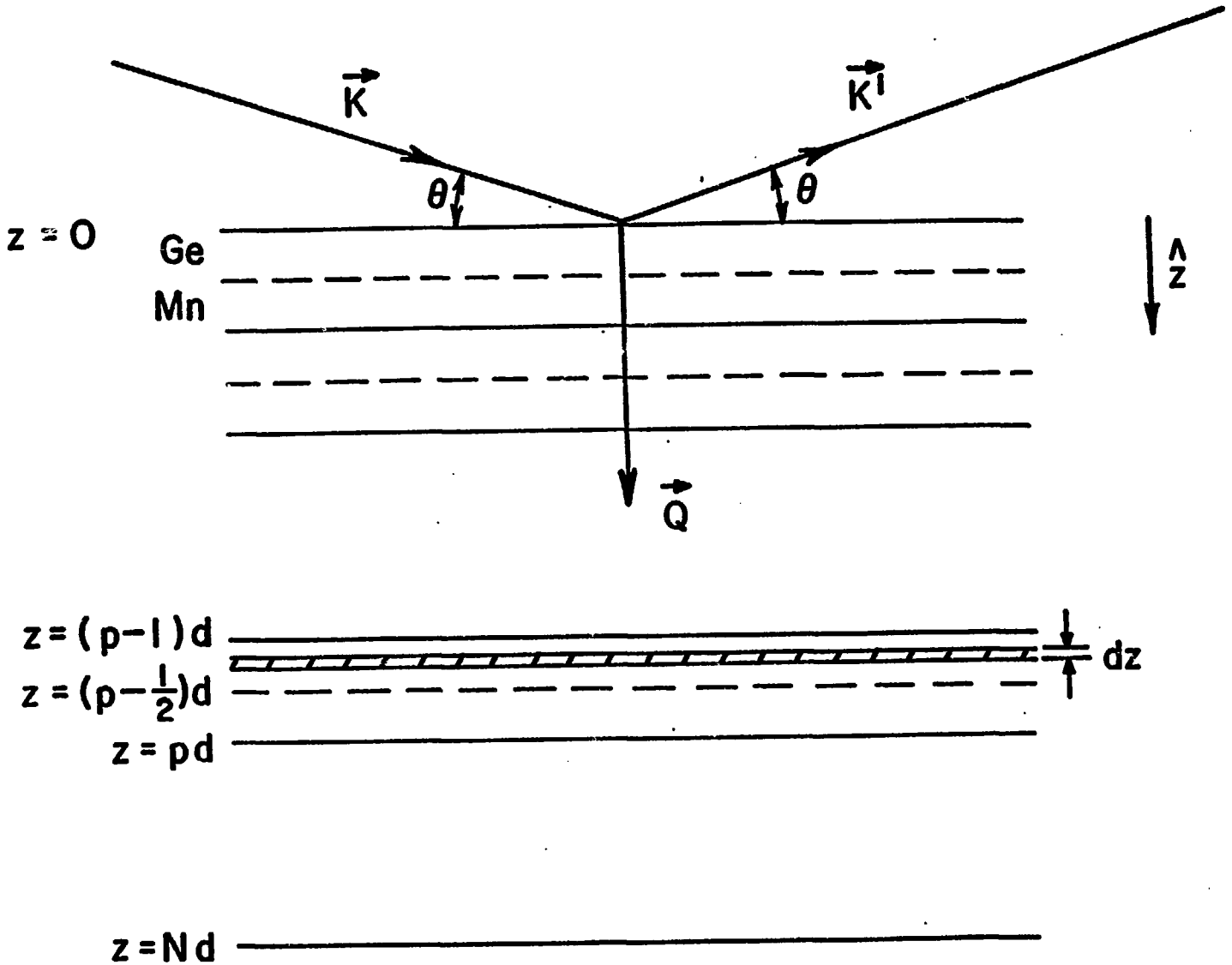

FIGURE 1

Fig. 1 (Neg. # 8-580-75)

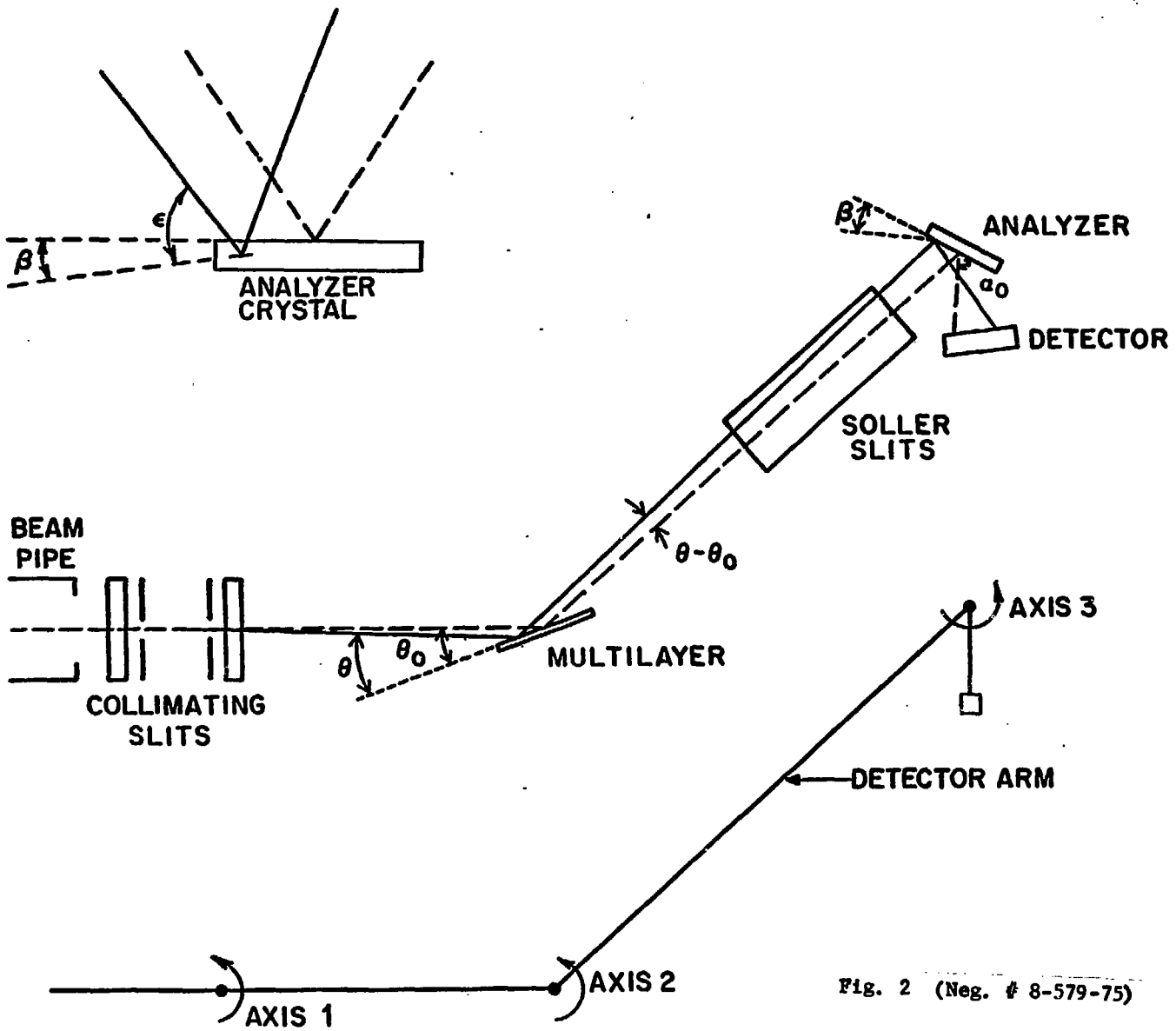

Fig. 2 (Neg. # 8-579-75)

FIGURE 2

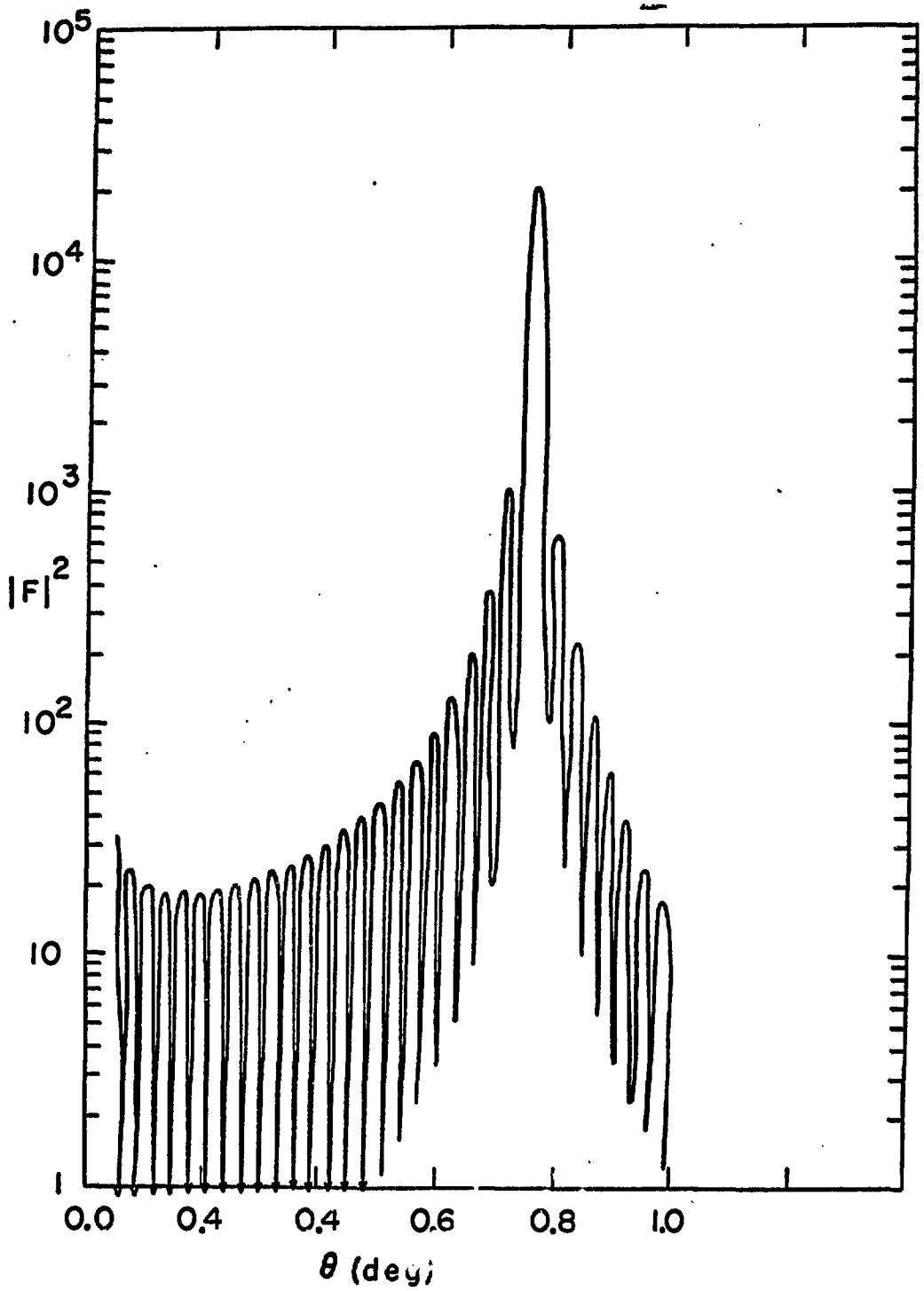

FIGURE 3 Fig. 3 (Neg. # 6-85-75)

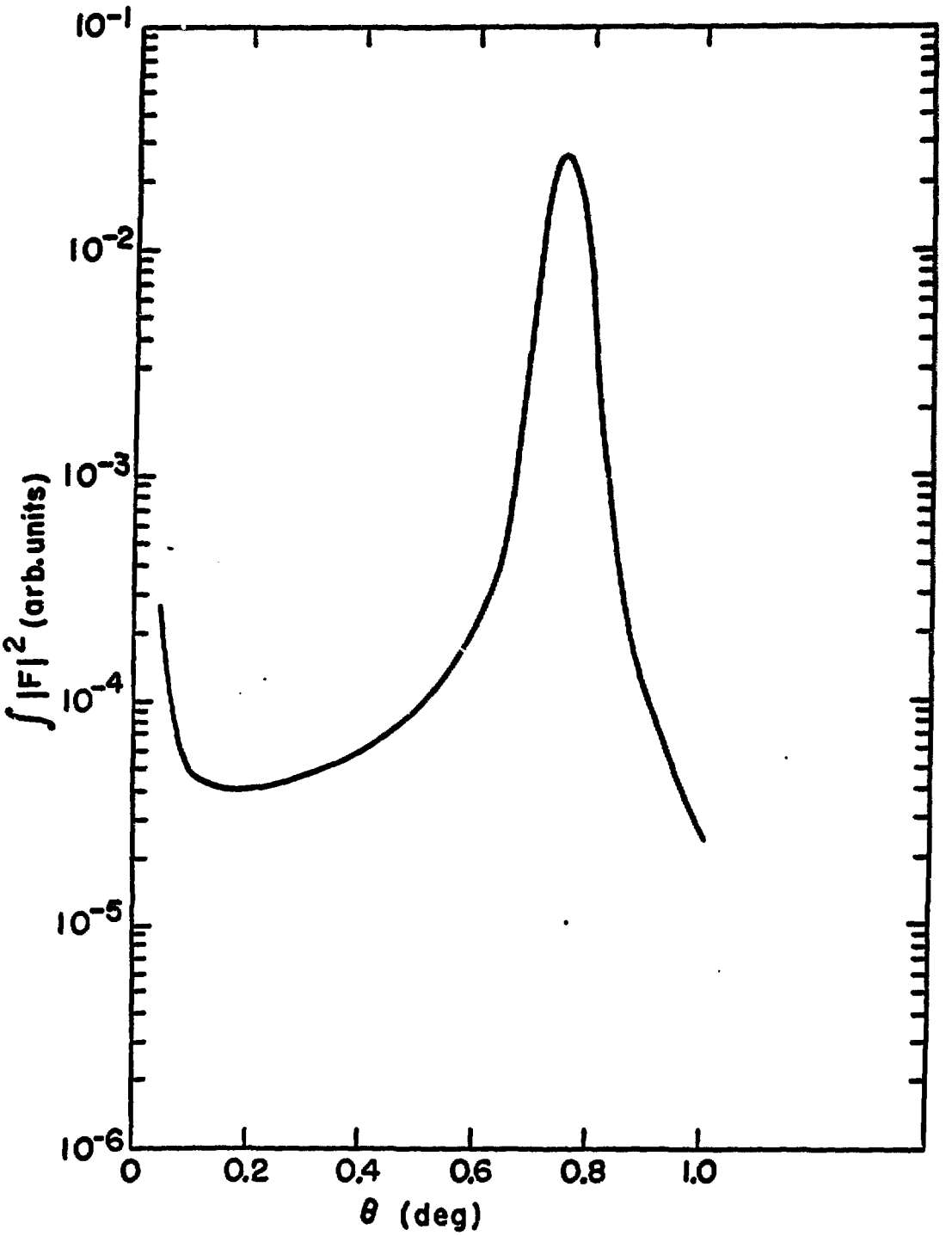

FIGURE 4

Fig. 4 (Neg. # 6-76-75)

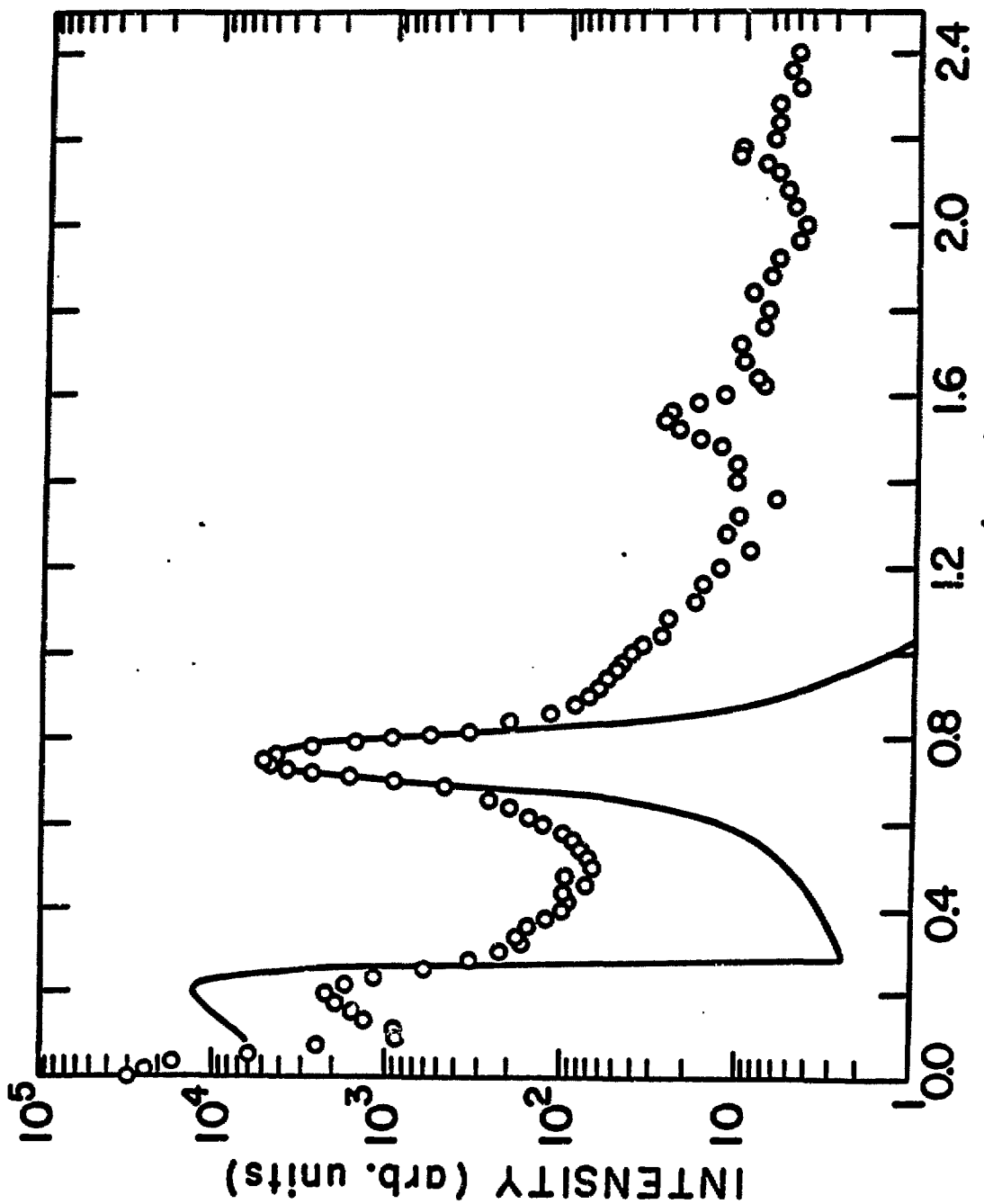

FIGURE 5

Fig. 5 (Neg. # 6-83-75)

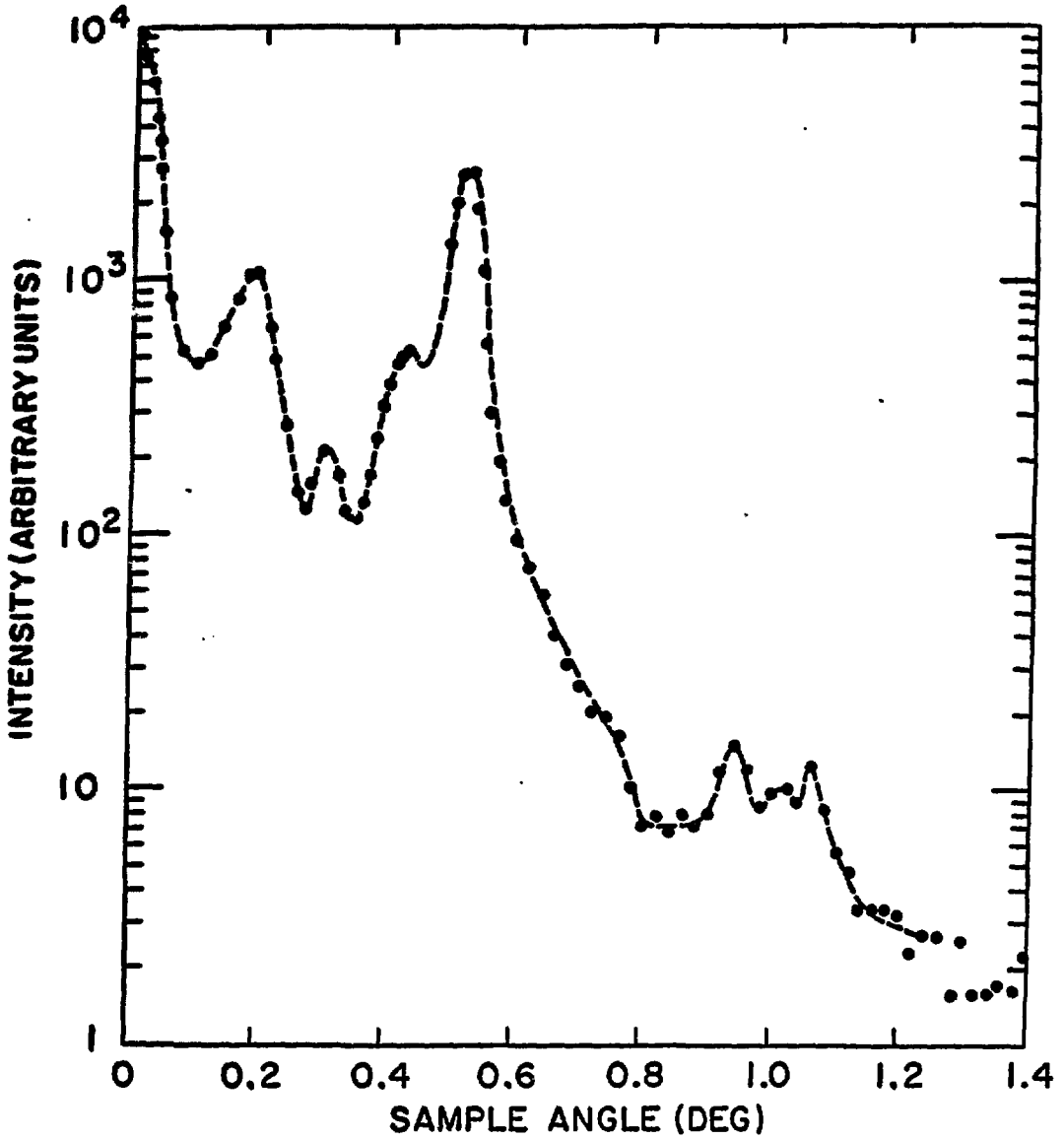

FIGURE 6

Fig. 6 (Neg. # 8-748-75)

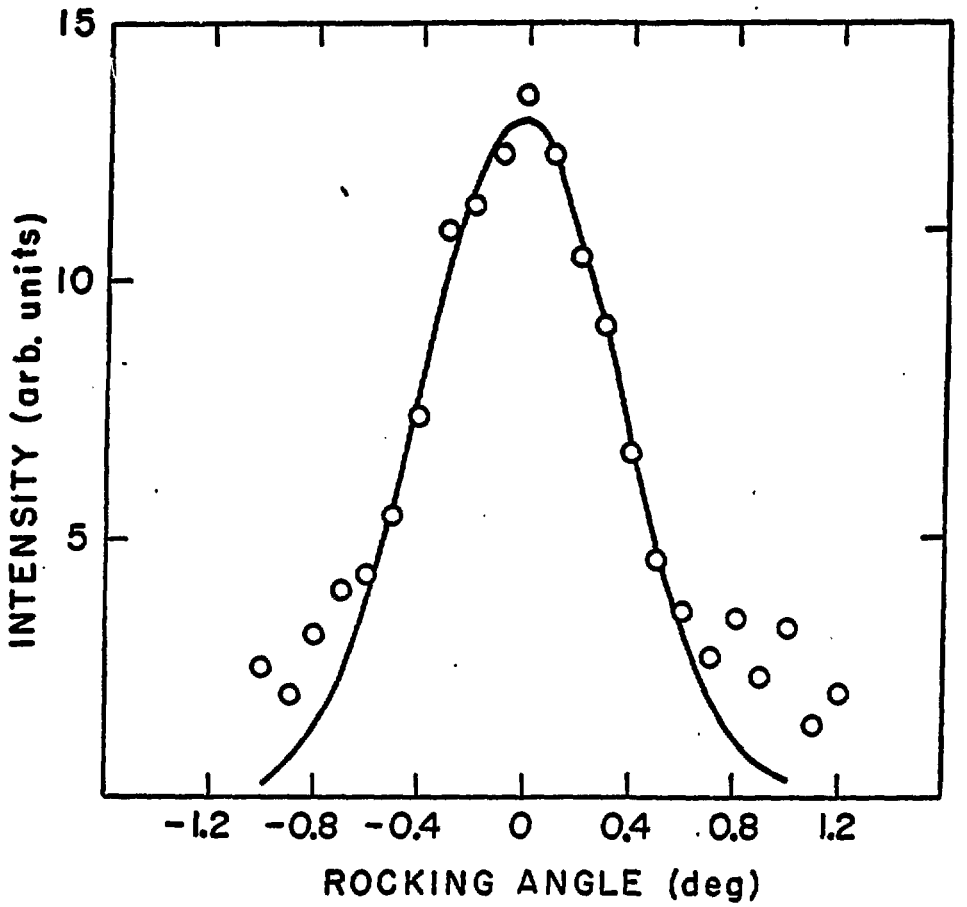

FIGURE 7

Fig. 7 (Neg. # 8-748-75)

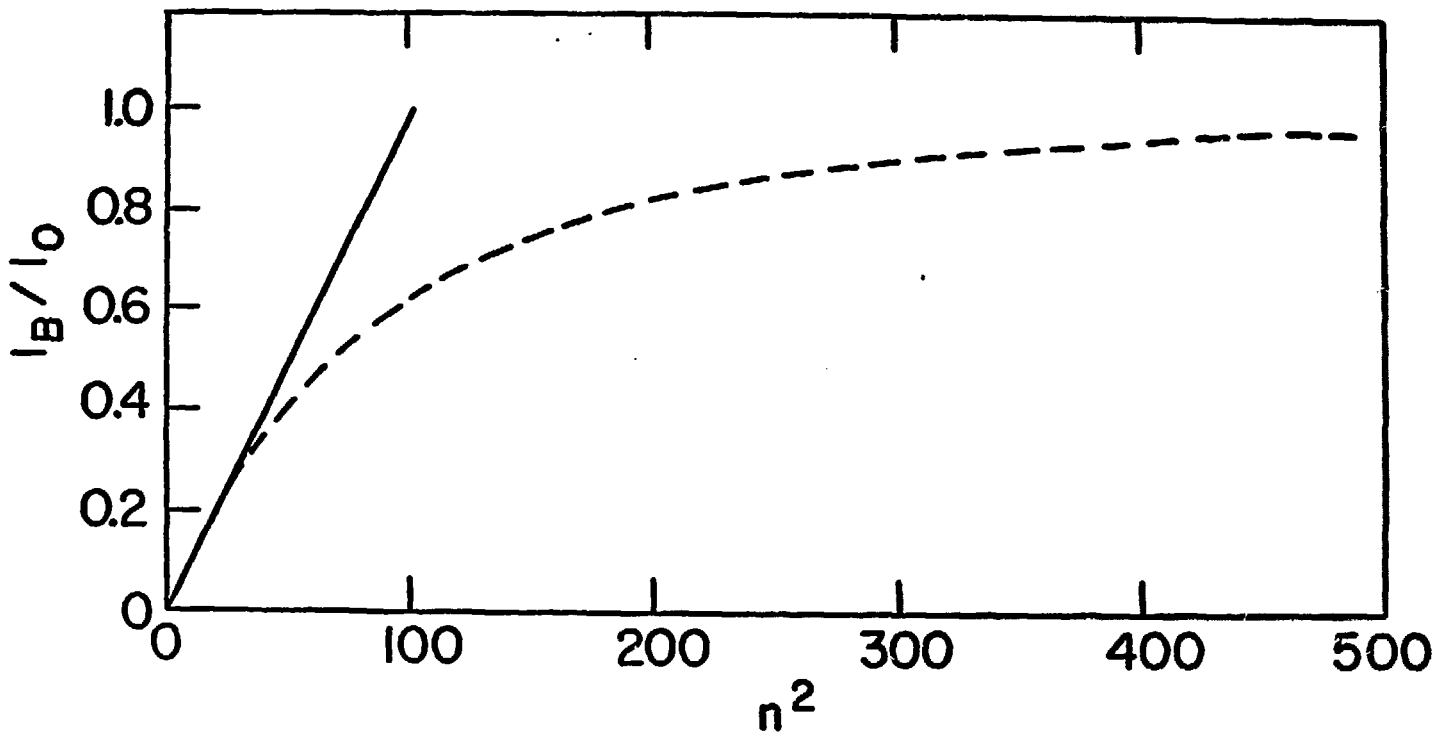

FIGURE 8

Fig. 8 (Neg. # 6-80-75)

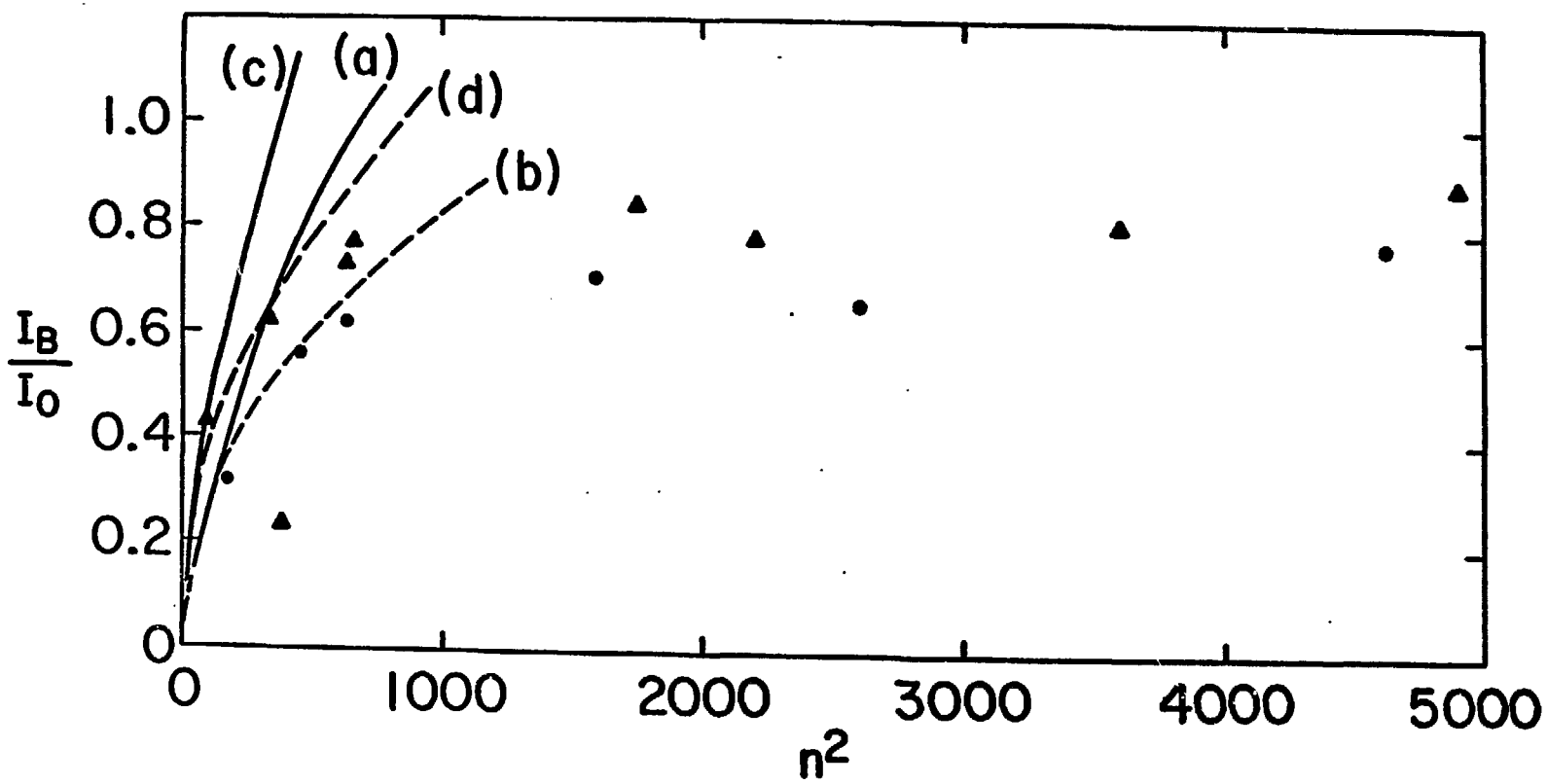

Fig. 9 (Neg. # 8-578-75)

FIGURE 9

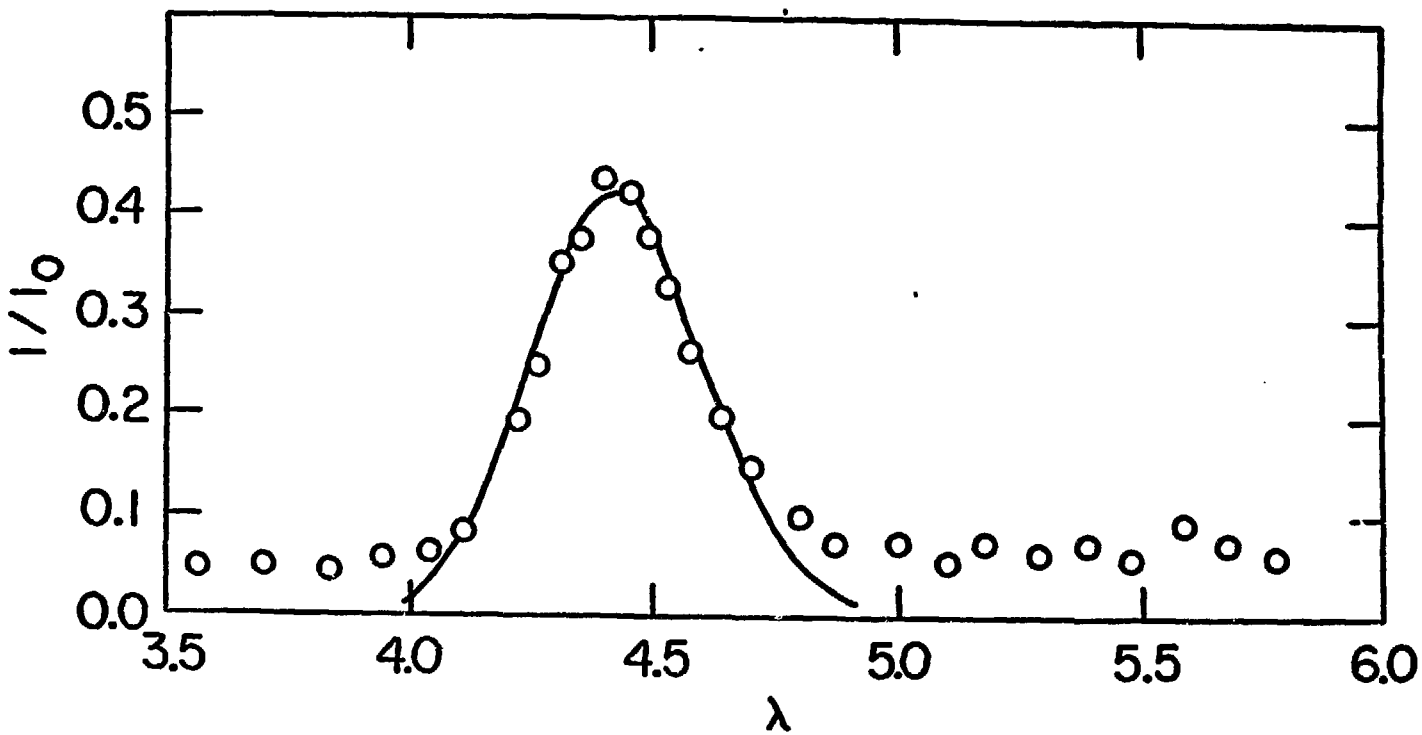

Fig. 10 (Neg. # 6-81-75)

FIGURE 10

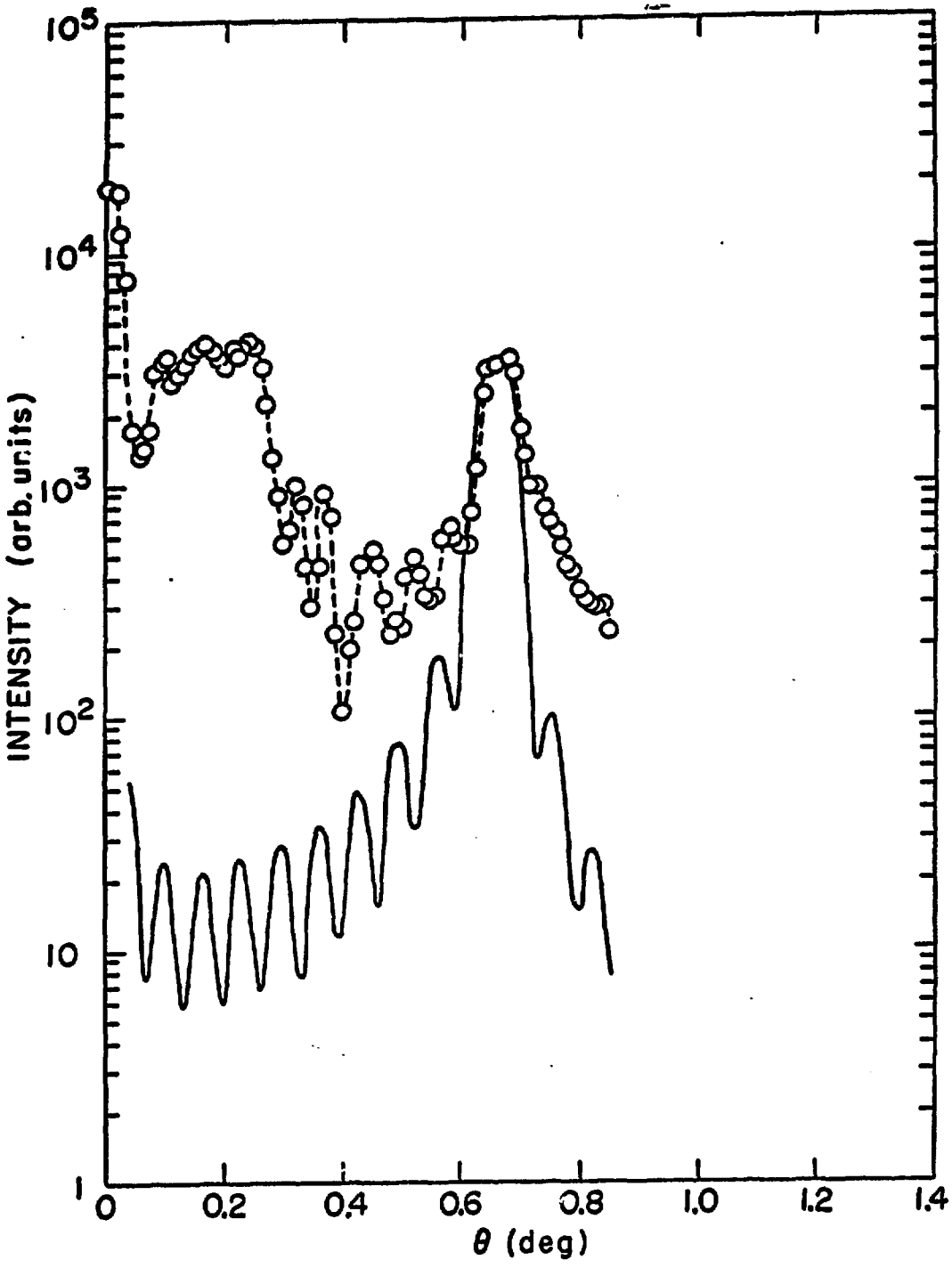

FIGURE 11

Fig. 11 (Neg. # 6-75-75)